J|A|C|S
ARTICLES
Published on Web 03/16/2002

The First Complete Identification of a Diastereomeric Catalyst−Substrate (Alkoxide) Species in an Enantioselective Ketone Hydrogenation. Mechanistic Investigations

Christopher J. A. Daley† and Steven H. Bergens*

Contribution from the Department of Chemistry, University of Alberta, Edmonton, Alberta T6G 2G2, Canada

Received February 2, 2001

Abstract: The enantioselective hydrogenations of the dialkyl 3,3-dimethyloxaloacetate ketone substrates (**2**, **3**, and **4**; alkyl = Me, ^{i}Pr, and ^{t}Bu, respectively) were catalyzed by [Ru((*R*)-BINAP)(H)(MeCN)$_n$(sol)$_{3-n}$](BF$_4$) (**1**, n = 0−3, sol = THF or MeOH, (*R*)-BINAP = (*R*)-2,2′-bis(diphenylphosphino)-1,1′-binaphthyl) in up to 82% ee (*R*). Reaction of the active catalyst **1** with 1 equiv of substrate (**2**, **3**, or **4**) in THF or MeOH solution formed the diastereomeric catalyst−alkoxide complexes [Ru((*R*)-BINAP)(MeCN)(OCH(CO$_2$R)(C(CH$_3$)$_2$CO$_2$R))](BF$_4$) (**5**/**6** R = Me, **8**/**9** R = ^{i}Pr, and **10** R = ^{t}Bu, respectively) via hydride addition to the ketone carbonyl carbon and ruthenium addition to oxygen. The absolute configurations at the alkoxide groups ((*R*)- for the major diastereomers **5**, **8**, and **10**) were determined via cleavage of the ruthenium−alkoxide bond with 1 equiv of HBF$_4$·OEt$_2$. The solution structures of the major diastereomer catalyst−alkoxide complexes (**5**, **8**, and **10**) were unambiguously determined by variable-temperature NMR spectroscopy. The major diastereomers (**5**, **8**, and **10**) had the same absolute configuration as the major product enantiomers from the catalytic hydrogenation of **2**, **3**, and **4** with **1** as catalyst. The ratio of major to minor alkoxide diastereomers was similar to the ee of the catalytic hydrogenation. The catalyst−alkoxide complexes are formed at temperatures as low as −30 °C with no other precursors or intermediates observed by NMR showing that ketone−hydride insertion is likely not the turnover limiting step of the catalytic hydrogenation. Results from the stoichiometric hydrogenolysis of **5**/**6**, **8**/**9**, or **10** indicate that their formation is rapid and only partially reversible prior to the irreversible hydrogenolysis of the ruthenium−oxygen bond. The stereoselectivities of the formation and hydrogenolysis of **5**/**6**, **8**/**9**, and **10** sum up to equal the stereoselectivities of the respective catalytic hydrogenations of **2**, **3**, and **4**. The rates of the hydrogenolysis were consistent with these diastereomers being true catalytic intermediates.

Introduction

We report the first complete and unambiguous structure determination of a diastereomeric catalyst−substrate complex (alkoxide) in an enantioselective ketone hydrogenation. The enantioselective catalytic hydrogenation of ketones is an extensively studied and utilized reaction.[1] Remarkable advances, especially by Noyori and co-workers, have recently been achieved in enantioselective ketone hydrogenations, including development of quite reactive catalyst systems[1a,2] that effect the highly enantioselective hydrogenations of keto esters,[1a,2l] of olefinic ketones,[1a,2h,i,p] of alkyl−aryl ketones,[1a,2e,f,o−q] and even of alkyl ketones.[2g,j,k,o−q] Despite these advances, and despite the many published studies of enantioselective ketone hydrogenations, *we know of no report describing the complete or unambiguous structural characterization of a diastereomeric ketone−catalyst compound, whether it is a putative catalytic intermediate or not.*[1a,3] As a result, the nature of the steric

* To whom correspondence should be addressed. E-mail: steve.bergens@ualberta.ca.

† Current address: Harvard University, 12 Oxford Street, Cambridge, MA, 02138.

(1) Examples of use in pharmaceuticals, industry, and academia: for a thorough, recent review, see: (a) Noyori, R.; Ohkuma, T. *Angew. Chem., Int. Ed.* **2001**, *40*, 40−73. Other examples include: (b) *Chirality in Industry*: Collins, A. N., Sheldrake, G. N., Crosby, J., Eds.; John Wiley & Sons: New York, 1997. (c) *Reductions in Organic Chemistry*: Abdel-Magid, A. F., Ed.; Adv. Chem. Ser. No. 641; American Chemical Society: Washington, DC, 1996. (d) Noyori, R. *Asymmetric Catalysis in Organic Synthesis*, Wiley: New York, 1994. (e) *Catalytic Asymmetric Synthesis*: Ojima, I., Ed.; VCH Publishers: New York, 1993.

(2) Selected examples of advances in enantioselective ketone hydrogenations. Ruthenium catalysts: (a) Ohkuma, T.; Ishii, D.; Takeno, H.; Noyori, R. *J. Am. Chem. Soc.* **2000**, *122*, 6510. (b) Mikami, K.; Korenaga, T.; Ohkuma, T.; Noyori, R. *Angew. Chem., Int. Ed.* **2000**, *39*, 3707. (c) Ohkuma, T.; Koizumi, M.; Ikehira, H.; Yokozawa, T.; Noyori, R. *Org. Lett.* **2000**, *2*, 659. (d) Noyori, R.; Ohkuma, T. *Pure Appl. Chem.* **1999**, *71*, 1493. (e) Mikami, K.; Korenaga, T.; Terada, M.; Ohkuma, T.; Pham, T.; Noyori, R. *Angew. Chem., Int. Ed. Engl.* **1999**, *38*, 495. (f) Cao, P.; Zhang, X. *J. Org. Chem.* **1999**, *64*, 2127. (g) Fehring, V.; Selke, R. *Angew. Chem., Int. Ed. Engl.* **1998**, *37*, 1827. (h) Ohkuma, T.; Koizumi, M.; Doucet, H.; Pham, T.; Kozawa, M.; Murata, K.; Katayama, E.; Yokozawa, T.; Ikariya, T.; Noyori, R. *J. Am. Chem. Soc.* **1998**, *120*, 13529. (i) Ohkuma, T.; Doucet, H.; Pham, T.; Mikami, K.; Korenaga, T.; Terada, M.; Noyori, R. *J. Am. Chem. Soc.* **1998**, *120*, 1086. (j) Nagel, U.; Roller, C. *Z. Naturforsch.* **1998**, *53b*, 267. (k) Doucet, H.; Ohkuma, T.; Murata, K.; Yokozawa, T.; Kozawa, M.; Katayama, E.; England, A. F.; Ikariya, T.; Noyori, R. *Angew. Chem., Int. Ed. Engl.* **1998**, *37*, 1703. (l) Ager, D. J.; Laneman, S. A. *Tetrahedron: Asymmetry* **1997**, *8*, 3327 and references within. (m) Genêt, J. P.; Ratovelomanana-Vidal, V.; Caño de Andrade, M. C.; Pfister, X.; Guerreiro, P.; Lenoir, J. Y. *Tetrahedron Lett.* **1995**, *36*, 4801. (n) Burk, M. J.; Harper, T. G. P.; Kalberg, C. S. *J. Am. Chem. Soc.* **1995**, *117*, 4423. (o) Ohkuma, T.; Ooka, H.; Ikariya, T.; Noyori, R. *J. Am. Chem. Soc.* **1995**, *117*, 10417. (p) Ohkuma, T.; Ooka, H.; Hashiguchi, S.; Ikariya, T.; Noyori, R. *J. Am. Chem. Soc.* **1995**, *117*, 2675. Rhodium catalyst: (q) Jiang, Q.; Jiang, Y.; Xiao, D.; Cao, P.; Zhang, X. *Angew. Chem., Int. Ed. Engl.* **1998**, *37*, 1100.

10.1021/ja0102991 CCC: $22.00

interactions within this scientifically and economically important enantioselective catalytic reaction can only be studied by using indirect experimental evidence.[1a,3,4]

Prior studies from this laboratory have demonstrated the utility of our catalyst system [Ru((*R*)-BINAP)(H)$(MeCN)_n(sol)_{3-n}$]-(BF_4) (**1**, BINAP is 2,2′-bis(diphenylphosphino)-1,1′-binaphthyl, $n = 0-3$, sol = MeOH, acetone, or THF depending on reaction medium) for the enantioselective hydrogenation of olefins.[5] This active catalyst is generated in high yields, in pure form, and it contains both a hydride and labile solvento ligands (eq 1). This

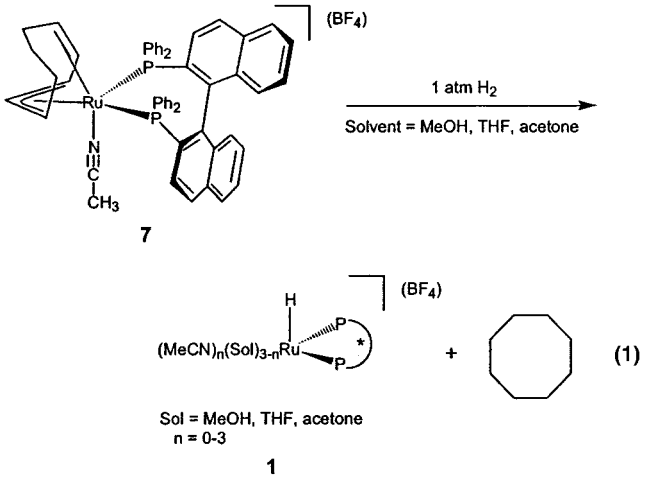

rare combination of features makes this system well-suited to study the mechanism of enantioselective hydrogenations.[6] For example, use of this system allowed the first isolation and X-ray structure determination of a diastereomeric catalyst−alkyl complex (formed by olefin−hydride insertion) of the same absolute configuration as the major product enantiomer of a catalytic olefin hydrogenation.[6a] Use of this system also allowed the first structure[7] determination of a diastereomeric olefin−catalyst adduct that contained a hydride ligand and that was of the same absolute configuration as the major product enantiomer. Observation was made at low temperatures of the diastereomeric olefin−hydride insertion by the olefin−catalyst adduct as a putative step in a catalytic olefin hydrogenation.[6c] The success obtained from use of **1** to study olefin hydrogenations has prompted us to extend its use to study the mechanism of enantioselective ketone hydrogenations.

In this study, we report our mechanistic investigations of the catalytic hydrogenations of the ketone substrates dimethyl, diisopropyl, and di-*tert*-butyl 3,3-dimethyloxaloacetate (**2**, **3**, and **4**) using **1** as catalyst (eq 2). We also report the solution-state

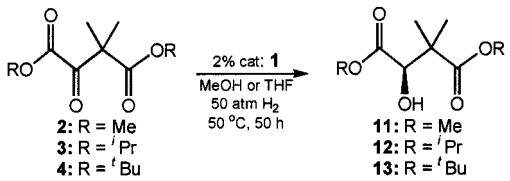

(2)

Substrate (Product)	ee (*R*) MeOH	ee (*R*) THF
2 (**11**)	59	59
3 (**12**)	68	66
4 (**13**)	82	80

structures of the major diastereomeric ketone−hydride insertion products between these substrates and **1**, the protonolysis of these alkoxides with $HBF_4 \cdot OEt_2$, and evidence for the mechanism of these catalytic hydrogenations.

Results and Discussion:

We chose ketones **2**, **3**, and **4** as substrates because they are nonenolizable and because they contain a distribution of functional groups that often results in high enantiomeric excess (ee) in catalytic hydrogenation: a 1,4-dicarbonyl unit with the prochiral functionality at the 2-position.[8] The catalytic hydrogenations of **2**, **3**, and **4** with **1** as catalyst (50 °C, 50 atm of H_2, 50 h) proceeded with complete conversion and with ee's ranging from moderate to good in MeOH (**2**, ee 59% (*R*); **3**, ee 68% (*R*), and **4**, ee 82% (*R*)) and in THF (**2**, ee 59% (*R*); **3**, ee 66% (*R*), and **4**, ee 80% (*R*)) (eq 2). The absolute configuration of all the major product enantiomers was the same (*R*), and the product ee increased as the steric bulk of the ester groups increased.

(3) Some partial characterization or identifications have been made. Two examples for rhodium systems: (a) Hatat, C.; Karim, A.; Kokel, N.; Mortreux, A.; Petit, F. *New J. Chem.* **1990**, *14*, 141. (b) Tani, K.; Tanigawa, E.; Tatsuno, Y.; Otsuka, S. *J. Organomet. Chem.* **1985**, *279*, 87. Three examples in ruthenium systems: (c) King, S. A.; DiMichele, L. In *Catalysis of Organic Reactions*; Scaros, M. G., Prunier, M. L., Eds.; Marcel-Dekker: New York, 1995; Vol. 62, p 157. (d) Mezzetti, A.; Tschumper, A.; Consiglio, G. *J. Chem. Soc., Dalton. Trans.* **1995**, 49. (e) Geraty, S. M.; Harkin, P.; Vos, J. G. *Inorg. Chim. Acta* **1987**, *131*, 217. Achiral ligand or substrate complexes: (f) Agbossou, F.; Carpentier, J.-F.; Hatat, C.; Kokel, N.; Mortreux, A. *Organometallics* **1995**, *14*, 2480. (g) Hayashi, Y.; Komiya, S.; Yamamoto, T.; Yamamoto, A. *Chem. Lett.* **1984**, 1363. (h) Hiraki, K.; Katayama, R.; Yamaguchi, K.; Honda, S. *Inorg. Chim. Acta* **1982**, *59*, 11. For structures of two catalytic intermediates (each not containing substrate) in Ru(II)-catalyzed transfer hydrogenations of ketones see: (i) Haack, K.-J.; Hashiguchi, S.; Fujii, A.; Ikariya, T.; Noyori, R. *Angew. Chem., Int. Ed. Engl.* **1997**, *36*, 285.

(4) Other mechanistic investigations of rhodium- and ruthenium-catalyzed enantioselective hydrogenation of ketones. Rhodium: (a) Agbossou, F.; Carpentier, J.-F.; Mortreux, A.; Surpateanu, G.; Welch, A. J. *New J. Chem.* **1996**, *20*, 1047. (b) Mezzetti, A.; Tschumper, A.; Consiglio, G. *J. Chem. Soc., Dalton Trans.* **1995**, 49. (c) Pasternak, H.; Pruchnik, F. P. *Polish J. Chem.* **1992**, *66*, 865. (d) Chiba, M.; Takahashi, H.; Morimoto, T.; Achiwa, K. *Tetrahedron Lett.* **1987**, *28*, 3675. (e) Torös, S.; Heil, B.; Kollar, L.; Marko, L. *Acta Chim. Hung.* **1985**, *119*, 135. (f) Ojima, I.; Kogure, T. *J. Organomet. Chem.* **1980**, *195*, 239. Ruthenium: (g) Abdur-Rashid, K.; Lough, A. J.; Morris, R. H. *Organometallics* **2000**, *19*, 2655. (h) Sánchez-Delgado, R. A.; Valencia, N.; Márquez-Silva, R.-L.; Andriollo, A.; Medina, M. *Inorg. Chem.* **1986**, *25*, 1106.

(5) (a) Wiles, J. A.; Lee, C. E.; McDonald, R.; Bergens, S. H. *Organometallics* **1996**, *15*, 3782. (b) Daley, C. J. A.; Wiles, J. A.; Bergens, S. H. *Can. J. Chem.* **1998**, *76*, 1447−1456.

(6) (a) Wiles, J. A.; Bergens, S. H. *J. Am. Chem. Soc.* **1997**, *119*, 2940. (b) Wiles, J. A.; Bergens, S. H. *Organometallics* **1998**, *17*, 2228. (c) Wiles, J. A.; Bergens, S. H. *Organometallics* **1999**, *18*, 3709.

(7) For examples of solution-state studies and structure determinations utilized in the investigation of other possible catalytic intermediates see: (a) van der Slot, S. C.; Kamer, P. C. J.; van Leeuwen, P. W. N. M.; Iggo, J. A.; Heaton, B. T. *Organometallics* **2001**, *20*, 430. (b) Hiraki, K.; Ishimoto, T.; Kawano, H. *Bull. Chem. Soc. Jpn.* **2000**, *73*, 2099. (c) Del Rio, I.; Pamies, O.; van Leeuwan, P. W. N. M.; Claver, C. *J. Organomet. Chem.* **2000**, *608*, 115. (d) Uriz, P.; Fernandez, E.; Ruiz, N.; Claver, C. *Inorg. Chem. Commun.* **2000**, *3*, 515. (e) Gridnev, I. D.; Higashi, N.; Asakura, K.; Imamoto, T. *J. Am. Chem. Soc.* **2000**, *122*, 7183. (f) Yi, C. S.; Lee, D. W. *Organometallics* **1999**, *18*, 5152. (g) van Rooy, A.; Kamer, P. C. J.; van Leeuwen, P. W. N. M. *J. Organomet. Chem.* **1997**, *535*, 201. (h) Giovannetti, J. S.; Kelly, C. M.; Landis, C. R. *J. Am. Chem. Soc.* **1993**, *115*, 4040. (i) McCulloch, B.; Halpern, J.; Thompson, M. R.; Landis, C. R. *Organometallics* **1990**, *9*, 1392. (j) Brown, J. M.; Maddox, P. J. *Chem. Commun.* **1987**, 1276. (k) Landis, C. R.; Halpern, J. *J. Am. Chem. Soc.* **1987**, *109*, 1746. (l) Brown, J. M.; Chaloner, P. A.; Morris, G. A. *Chem. Commun.* **1983**, 664. (m) Brown, J. M.; Murrer, B. A. *J. Chem. Soc., Perkin Trans. 2* **1982**, 489. (n) Brown, J. M.; Chaloner, P. A. *J. Chem. Soc., Perkin Trans. 2* **1982**, 711. (o) Brown, J. M.; Chaloner, P. A.; Glaser, R.; Geresh, S. *Tetrahedron* **1980**, *36*, 815. (p) Brown, J. M.; Chaloner, P. A. *Chem. Commun.* **1980**, 344. (q) Brown, J. M.; Chaloner, P. A. *J. Am. Chem. Soc.* **1980**, *102*, 3040. (r) Brown, J. M.; Chaloner, P. A. *Chem. Commun.* **1979**, 613.

(8) This arrangement is found in commonly utilized α,β-unsaturated acid substrates and their derivatives (e.g. itaconic acid/esters and α-acetamido-cinnamic acid/esters) for highly enantioselective catalytic hydrogenations.

We carried out stoichiometric reactions between **2** and the active catalyst **1** at room temperature in THF and MeOH to investigate the mechanism of these ketone hydrogenations. These reactions resulted in the immediate loss of hydride signal[9] in the ^{1}H NMR spectrum with concomitant formation of two species (**5** and **6**, in a 79.5:20.5 ratio) of similar NMR representation, suggesting they were diastereomeric catalyst−alkoxides (eq 3). The corresponding reaction between the

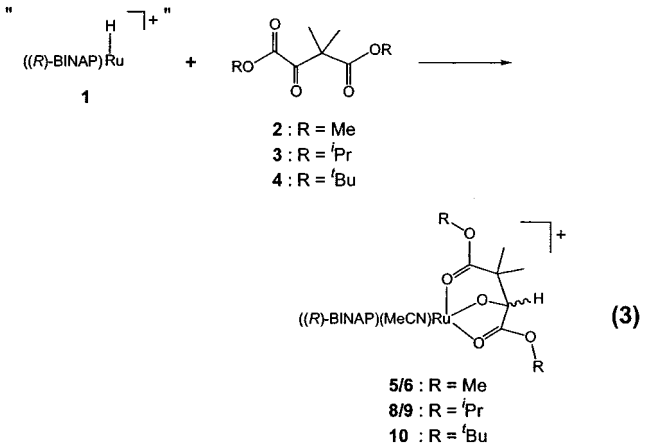

(3)

diisopropyl ester (**3**) and the active catalyst **1** was also complete on mixing at room temperature to form the major and minor product diastereomers (**8** and **9**) in a 90:10 ratio. The same reaction with the bulky di-*tert*-butyl ester **4** formed exclusively the product diastereomer **10**.

It was imperative to determine the structures of **5**, **6**, **8**, **9**, and **10** to confirm that ketone−hydride insertion occurred, and to investigate the steric interactions within these possible catalytic intermediates. Attempts to obtain crystals suitable for structure determination by X-ray diffraction of **5**, **6**, or any of the catalyst−substrate complexes reported in this manuscript were unsuccessful. NMR and isotope labeling experiments were used instead to obtain the solution-state structures of these species.

Characterization of Catalyst-Substrate Species. (a) Broad Structural Features. NMR experiments showed that **5** and **6** were ruthenium−alkoxide diastereomers resulting from ketone−hydride insertion with hydride addition to carbon and ruthenium addition to oxygen (eq 3). Specifically, the signals for the alkoxy protons (RuOC*H*−) were identified as the overlapping peaks at δ 3.84 (br s) in the ^{1}H NMR spectrum as follows. HMQC experiments showed these signals correlated to the overlapping signals at δ 87 in the ^{13}C NMR spectrum. HMBC experiments indicated the peaks at δ 87 arose from the alkoxy carbon centers. We synthesized the deuterium-labeled diastereomers $\mathbf{5}_{(\mathrm{RuOC}D-)}$ and $\mathbf{6}_{(\mathrm{RuOC}D-)}$ by reaction of **2** with **1**-d_1 (**1**-d_1 is obtained by reaction of [Ru((*R*)-BINAP)(1-3;5-6-η-C_8H_{11})(MeCN)](BF$_4$) (**7**) with deuterium gas).[6b] This substitution resulted in loss of the alkoxide signal at δ 3.84 in the ^{1}H NMR spectrum of the product, and inversion of the signal at δ 87 in ^{13}C APT NMR experiments (Scheme 1), proving that these signals correspond to the proton and the carbon atom of the alkoxide, respectively. These experiments unambiguously identify the products of the reaction between **2** and **1** as ruthenium−alkoxides resulting from rapid, exergonic ketone−hydride insertion.

Scheme 1. Test for Ruthenium−Alkoxide Formation[a]

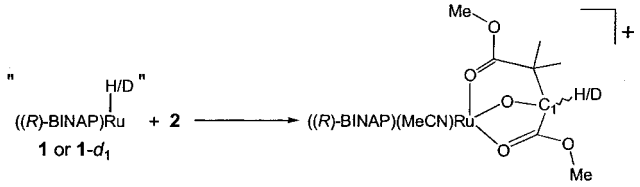

[a] As expected, the ^{13}C APT signal of C_1 is inverted with respect to the reaction **1** + **2** (C_1-H forms) versus **1**-d_1 + **2** (C_1-D forms).

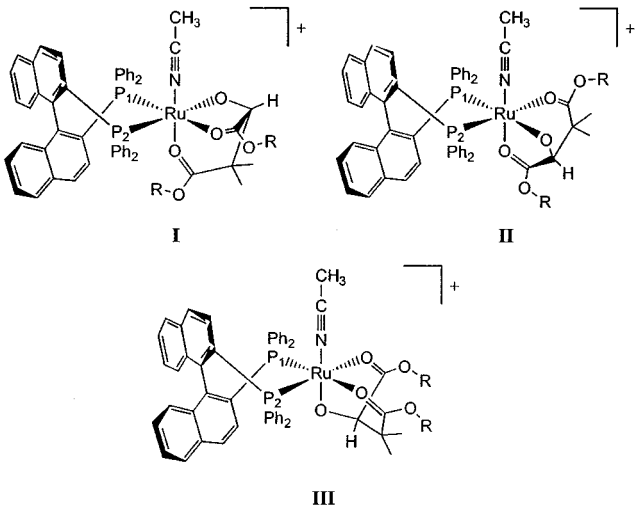

Figure 1. The three possible structures (**I**, **II**, and **III**) of the major diastereomer formed from reaction of **1** with **2**, **3**, or **4**.

The remaining assignments of the broad structural features were completed as follows. Both ester groups were bonded to ruthenium as shown by ^{13}C−^{31}P coupling in the ^{13}C{^{1}H} NMR spectra. The coupling constants were similar for both ester groups and ranged from 2 to 3 Hz, making it impossible to determine with ^{13}C−^{31}P coupling which of the ester groups were trans to a phosphorus center. The presence of a single coordinated MeCN ligand was confirmed by ^{1}H NMR and by ^{15}N NMR of the ^{15}N-labeled isotopomer. The signals in the ^{31}P NMR spectra of the ^{15}N-labeled MeCN isotopomers of **5** and **6** had only small ^{31}P−^{15}N coupling constant (**5**: $^2J_{\mathrm{P-N}} = 2.8$ Hz; **6**: $^2J_{\mathrm{P-N}} = 2.9$ Hz), showing that the MeCN ligand occupied a coordination site mutually cis to both phosphorus centers.[10] These data prove that diastereomers **5** and **6** contain one MeCN ligand, and they contain **2** as a tridentate alkoxide ligand bonded to ruthenium in a *fac* arrangement through the ester carbonyl groups and the alkoxide group (Figure 1: shown for one diastereomer). Such *fac*-tridentate bonding by the alkoxide of **2** is expected as molecular models suggest the alkoxide cannot readily adopt a *mer*-tridentate arrangement about ruthenium.

The magnitudes of the ^{31}P NMR chemical shifts and coupling constants for the major diastereomers (**5**, **8**, and **10**) formed by the ketone−hydride insertion were similar. Further, the magnitudes of $^3J_{\mathrm{P-C}}$ (2 to 3 Hz) for the ester carbonyls and the

(9) King et al. (ref 3c) reported similar observations for reaction between β-keto esters and the partially characterized hydrides obtained from hydrogenation of Ru(BINAP)(Cl)$_2$/NEt$_3$ in CH_2Cl_2. The products reported by King were the corresponding β-hydroxy ester and unidentified ruthenium complexes.

(10) We have shown previously (ref 6c) in the related complex [Ru((*R*)-BINAP)(H)(^{15}N-MeCN)$_3$]$^+$ that only when MeCN is coordinated trans to phosphorus in these complexes does it show significant ^{31}P−^{15}N coupling ($^2J_{\mathrm{P-N}} \geq 8$ Hz).

magnitudes of $^2J_{P-N}$ ($\sim$ 3 Hz) in the ^{15}N-labeled isotopomers of **8**, **9**, and **10** all showed that the alkoxide ligands in these complexes bind to ruthenium in a tridentate manner with a *fac* arrangement of the ester carbonyl and alkoxide groups. Thus the major diastereomers formed by the ketone−hydride insertion have the same broad structural features (Figure 1).

(b) Absolute Configurations. The absolute configurations at the alkoxide carbon centers were determined by protolytic cleavage of the ruthenium−alkoxide bond in $\mathbf{5}_{(RuOCD-)}$ and $\mathbf{6}_{(RuOCD-)}$ with $HBF_4{\cdot}OEt_2$ at room temperature in CH_2Cl_2. The protonolysis is complete upon mixing to generate the dicationic adducts [Ru((*R*)-BINAP)(MeCN)((*R* and *S*)-$MeCO_2CD(OH)C(Me)_2CO_2Me$)]$(BF_4)_2$. Addition of excess MeCN liberated $MeCO_2CD(OH)C(Me)_2CO_2Me$ (**11**-d_1) and formed the known dicationic ruthenium compound [Ru((*R*)-BINAP)$(MeCN)_4$]$(BF_4)_2$ (**14**, eq 4).[11] No H−D exchange occurred at the alkoxide

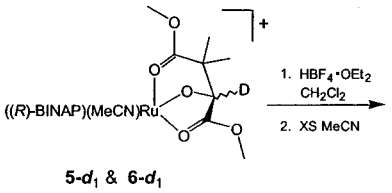

5-d_1 & **6**-d_1

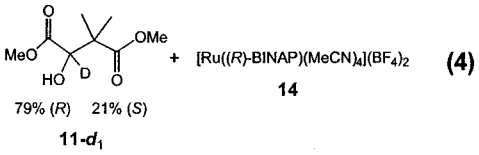

11-d_1 **(4)**

carbon of the product, showing that epimerization did not occur during the protonolysis. Furthermore, the ee of the liberated alcohol **11**-d_1 was 60% (*R*), which corresponds to the ratio of $\mathbf{5}_{(RuOCD-)}$ to $\mathbf{6}_{(RuOCD-)}$ used for this experiment (CH_2Cl_2 solution; 80:20). Combined, the results from protonolysis of $\mathbf{5}_{(RuOCD-)}$ and $\mathbf{6}_{(RuOCD-)}$ unambiguously assign the absolute configuration of the major alkoxide diastereomer **5** as *R*, and that of the minor diastereomer **6** as *S*. Protonolysis of a 90:10 mixture of $\mathbf{8}_{(RuOCD-)}$ and $\mathbf{9}_{(RuOCD-)}$ generated (after liberation by MeCN) the alcohol ^{i}PrCO$_2$C*D*(OH)C(Me)$_2$CO$_2{}^i$Pr (**12**-d_1) in 79% ee (*R*) without observable H−D exchange. Finally, protonolysis of the exclusively formed diastereomer $\mathbf{10}_{(RuOCD-)}$ generated (after liberation by MeCN) (*R*)-^{t}BuCO$_2$C*D*(OH)C(Me)$_2$CO$_2{}^t$Bu (**13**-d_1) exclusively, without observable H−D exchange. In each case, the observed ee corresponds to the observed diastereomeric excess (de) of the respective alkoxide intermediates. The major diastereomer of the catalyst−alkoxide complex formed by reaction of **2**, **3**, or **4** with the active catalyst **1** therefore contains the (*R*)-alkoxide in all cases. This absolute configuration matches that of the major product enantiomer of the catalytic hydrogenation of these substrates.

(c) Fine Structural Features. Figure 1 shows the only three possible isomers of the major ruthenium−alkoxide diastereomers **5**, **8**, and **10** that are consistent with the absolute configuration and the bulk structural features determined thus far (vide supra). They are all of *R* absolute configuration at the alkoxy carbon, the MeCN ligand is in a coordination site cis to both phosphorus centers, and the substrate is bonded to ruthenium as a tridentate ligand through the alkoxy and ester carbonyl oxygen atoms.

(11) Mashima, K.; Hino, T.; Takaya, H. *J. Chem. Soc., Dalton Trans.* **1992**, 2099.

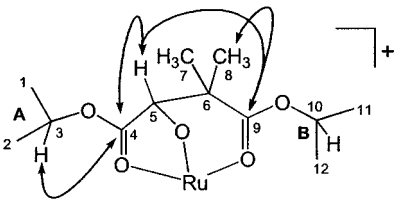

Assignment	^{1}H NMR (δ)	^{13}C NMR (δ)
1 or 2	0.76	20 (overlap)
1 or 2	1.15	21 (overlap)
3	4.76	73
4	---	190
5	3.82	87
6	---	46
7 or 8	0.8	24
7 or 8	0.98	21 (overlap)
9	---	182
10	5.42	72
11 or 12	1.09	18
11 or 12	1.23	20 (overlap)

Figure 2. Assignments of substrate ^{1}H and ^{13}C NMR signals of **8** along with key HMBC correlations (shown by arrows to structure).

They differ by which coordination sites are occupied by the alkoxide and ester groups. In diastereomer **I** the alkoxy group is coordinated trans to P_2, the phosphorus center attached to the naphthyl ring on the same side of the P_1-Ru-P_2 plane as the MeCN ligand; in **II** the alkoxy group is coordinated trans to P_1, the phosphorus center attached to the naphthyl ring on the opposite side of the P_1-Ru-P_2 plane as the MeCN ligand; and in **III** the alkoxy group is coordinated cis to both phosphorus centers. Overlap of signals in the ^{1}H and ^{13}C NMR spectra of the diastereomers **5** and **6** prevented us from obtaining unambiguous correlation data to distinguish between **I**, **II**, or **III**. Such overlap was minimal for diastereomers **8** and **9** because the corresponding minor diastereomers were present in low concentrations. The completed characterization of the major diisopropyl diastereomer **8** is described below.

(d) Substrate Signals. Figure 2 shows these assignments. Analysis of the COSY and selective ^{1}H{^{1}H} decoupling data assigned by correlation the signals from the protons in each isopropyl group (isopropyl A: δ 0.76 and 1.15—methyl groups, and δ 4.76—methyne proton; isopropyl B: δ 1.09 and 1.23—methyl groups, and δ 5.42—methyne proton). Analysis of the HMQC data identified the ^{13}C signals that corresponded to the isopropyl methyne carbons, the alkoxy carbon, and the methyl groups on the backbone of the coordinated substrate (Figure 2; carbons 3 and 10; 5; and 7 and 8, respectively). With these assignments, the analysis of the HMBC data showed that the alkoxide methyne proton coupled to both ester carbonyl carbon signals at δ 182 and 190. Further, the backbone methyl groups coupled with only the ester carbonyl carbon signal at δ 182, unambiguously assigning it to the ester carbonyl group β to the alkoxide unit (carbon 9), and assigning the remaining carbonyl carbon signal (δ 190) to the α ester carbonyl group (carbon 4). HMBC data also showed that the methyne proton signal from the isopropyl unit A (δ 4.76) coupled to the α ester carbonyl carbon (δ 190).[12] Therefore isopropyl unit B is that

(12) The methyne proton signal of isopropyl group B (δ 5.42) did not show any correlation to either ester carbonyl carbon signal (by HMBC experiments), that the methyne proton signal of isopropyl group A (δ 4.76) did is sufficient proof of assignments.

^{31}P-^{1}H HETCOR	
Assignment	^{1}H NMR (δ)
P_1-*ortho*-Naph	7.02 (r.t.)
P_1-*ortho*-Ph_{ax}	9.15/6.19 (-100 °C)
P_1-*ortho*-Ph_{eq}	7.15/7.95 (-40 °C)
P_2-*ortho*-Naph	8.02 (r.t.)
P_2-*ortho*-Ph_{ax}	8.76/7.05 (-40 °C)
P_2-*ortho*-Ph_{eq}	7.64 (r.t)

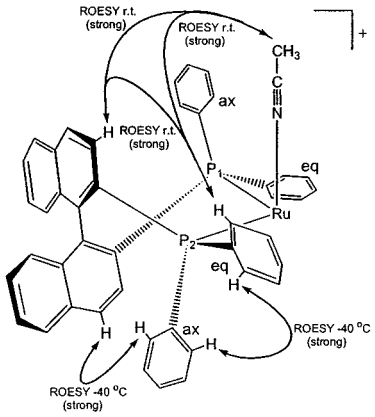

Figure 3. Assignment of ortho protons on the phenyl and naphthyl rings bonded to P_1 and P_2 from ^{31}P−^{1}H HETCOR and variable-temperature ROESY data. The quadrant of space about the ruthenium center was identified.

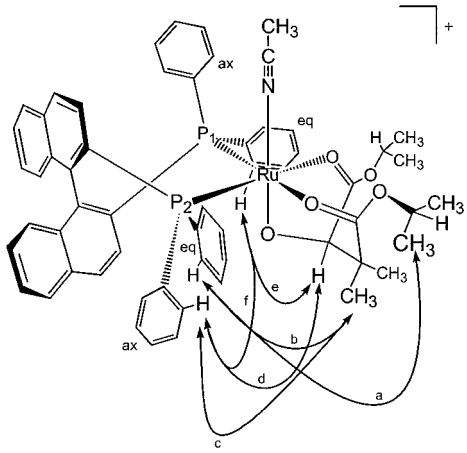

Figure 4. Important ROE contacts observed between the substrate and (*R*)-BINAP ligand at ambient-temperature to −40 °C (a, b, and c; all strong) and key ROE contacts at −80 °C (d, e, and f; all strong) that conclusively identified **III** as the structure of **8** (as well as for **5** and **10**).

of the β ester group. Similar assignments were made for the substrate unit in both the dimethyl major diastereomer **5** and the di-*tert*-butyl diastereomer **10**, except that for **10** the HMBC experiments could not distinguish the *tert*-butyl group ^{1}H NMR signals to the α or β ester groups due to the limits of detection.[13]

(e) BINAP Signals and Correlations. Figure 3 shows the conformation of coordinated (*R*)-BINAP and the spatial distribution of its components relative to the cis-coordinated MeCN ligand. The relative tilt of the naphthyl rings forces one phenyl ring of each phosphorus axial and the other equatorial. Placing MeCN in the cis-coordination site shown in Figure 3 orients the P_2 axial phenyl (P_2−Ph_{ax}) ring on the opposite side of the P_1−Ru−P_2 plane as MeCN, and the naphthyl group (P_2−Naph) on the same side of the plane as MeCN. Consequently, P_1−Ph_{ax} is on the same side of the P_1−Ru−P_2 plane as MeCN and P_1−Naph is opposite. As (*R*)-BINAP is C_2-symmetric, it is of no consequence which side of the P_1−Ru−P_2 plane the MeCN ligand is initially placed for this assignment of structure. The choice shown in Figure 3 was arbitrary.

Variable-temperature ^{31}P−^{1}H HETCOR experiments assigned the ^{1}H NMR signals to the ortho protons on the phenyl and naphthyl rings bonded to P_1 and P_2 (Figure 3). Each ^{31}P signal will show from three (with rapid rotation about the P−phenyl bond) to five (with slow rotation about the P−phenyl bond) ^{1}H correlations with the two axial *o*-phenyl protons, with the two equatorial *o*-phenyl protons, and with the one *o*-naphthyl proton. Ambient-temperature studies identified only two ^{1}H correlations to P_2 and one ^{1}H correlation to P_1, showing that rotation about most of the phosphorus−phenyl bonds was rapid at room temperature, and that some *o*-phenyl ^{1}H NMR signals were in the baseline of the spectrum. Indeed, variable low-temperature investigations (−40 to −100 °C) were required to identify all the ortho protons. Some of these signals only grew out of the baseline at −80 °C, suggesting that rotation about the P−phenyl bond can be quite facile in BINAP complexes.

Figure 3 shows assignments of the BINAP-MeCN and BINAP-BINAP correlations. Ambient-temperature ROESY experiments showed a ROE contact between C*H*$_3$CN and only one *o*-naphthyl signal (δ 8.02). This ortho proton must therefore be on the naphthalene ring bonded to P_2 and on the same side of the ruthenium−phosphine plane as CH_3CN (Figure 3, P_2−*o*-Naph). This P_2−*o*-Naph ^{1}H signal also showed a ROE contact at ambient-temperature to the ^{1}H signal (δ 7.64) from two *o*-phenyl protons associated with P_2. This signal is thereby unambiguously assigned to the equatorial P_2 *o*-phenyl protons as they are the only ortho protons close to the P_2−*o*-Naph proton. Finally, the ^{1}H NMR signal for the P_1−*o*-Naph proton was found at δ 7.02. The signals of both P_1−*o*-Ph_{ax} (observed at <−40 °C) and P_1−*o*-Ph_{eq} (observed at <−80 °C) were identified by ^{31}P−^{1}H HETCOR studies and ROESY studies at low temperatures that are described further below.

Having identified the absolute configuration at the alkoxide group, and having assigned the NMR signals to key substrate and BINAP elements, it was possible to use low-temperature ROESY experiments to unambiguously assign the structure of the major diastereomer. At −40 °C, the backbone methyl group proton signals (δ 0.8, Figure 4, correlations b and c) showed ROE contacts to the P_2−*o*-Ph_{eq} (δ 7.64) and the P_2−*o*-Ph_{ax} (δ 8.76) proton signals. Thus one backbone methyl group is close to both the P_2 axial and equatorial phenyl rings. Further, the methyne proton and one of the methyl group protons of isopropyl unit B showed ROE contacts to P_2−*o*-Ph_{eq} (Figure 4, correlation a), showing this group is proximal to P_2 as well.

At −80 °C the alkoxy methyne proton (δ 3.85) had ROE contacts with the P_2−*o*-Ph_{ax} (Figure 4, correlation d) as well as with a P_1−*o*-Ph_{eq} proton (δ 9.15, Figure 4, correlation e).[14] Inspection of molecular models shows that the only alkoxide diastereomer (of **I**, **II**, or **III** (Figure 1)) with the alkoxy methyne proton in proximity to P_2−Ph_{ax} and P_1−Ph_{eq}, with the isopropyl unit B in proximity to P_2−Ph_{eq}, and with a backbone methyl group in proximity to P_2−Ph_{eq} and P_2−Ph_{ax} is **III** (Figure 4). This assignment is unambiguous. The major diastereomers of

(13) The experimental limits of detection of the HMBC NMR experiment are generally 3-bond correlations. The *tert*-butyl methyl protons are four bonds away from their respective ester carbonyl carbon atoms and thus correlations were not observed.

(14) The signal at δ 9.15 was assigned to a P_1−*o*-Ph_{eq} proton as follows. ^{31}P−^{1}H HETCOR experiments carried out at −100 °C showed correlation to P_1. ROESY experiments carried out at −80 °C showed a ROE contact with P_2−*o*-Ph_{ax} (Figure 4, correlation f). The only *o*-phenyl protons attached to P_1 that are in proximity to P_2−*o*-Ph_{ax} are P_1−*o*-Ph_{eq} as the P_1−*o*-Ph_{ax} protons are on the opposite side of the P_1−Ru−P_2 plane (Figure 4). This signal showed exchange (−80 °C) with the ^{1}H NMR signal at δ 6.2 indicating that the latter arises from the other P_1−*o*-Ph_{eq} proton exchanged by rotation about the P_1−Ph_{eq} bond. The remaining P_1−*o*-phenyl protons were then assigned to P_1−*o*-Ph_{ax} (δ 7.15 and 7.95 at − 40 °C) as they were the only ones left unassigned.

the hydride insertion reactions between **1** and the ketones **2**, **3**, and **4** all therefore have the solution-state structure **III**.[15] These species are of the same absolute configuration as the major product enantiomer of the catalytic hydrogenation. Further experiments were carried out to investigate whether these species were true catalytic intermediates.

Low-Temperature Studies. Stoichiometric reactions between **1** and each of the ketone substrates **2**, **3**, and **4** in THF-d_8 were carried out at low temperatures and monitored by NMR spectroscopy to investigate the ketone−hydride insertion (eq 5). No evidence of reaction was observed below −30 °C. The

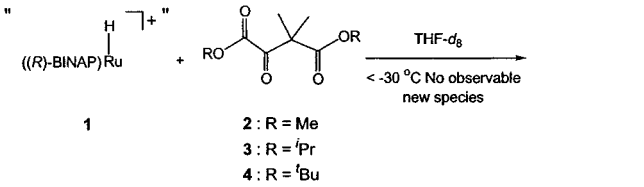

1 **2** : R = Me; **3** : R = ^{i}Pr; **4** : R = ^{t}Bu

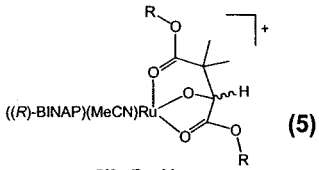

(5)

5/6 : R = Me; **8/9** : R = ^{i}Pr; **10** : R = ^{t}Bu

insertion begins at −30 °C to form the ruthenium−alkoxide diastereomers (**5**/**6**, **8**/**9**, and **10**) *without* other observable intermediates. Assuming ketone−hydride insertion in these systems is analogous to olefin−hydride insertion, in that it requires prior coordination of the ketone as an η^2-π-ligand cis to the hydride,[16] these results show that ketone coordination is slower than ketone−hydride insertion in this system. An intriguing alternative is that this "insertion" reaction proceeds via nucleophilic attack of the hydride ligand on the carbonyl carbon. Such a process would not require coordination of the ketone to ruthenium and would be facilitated by coordination of the ester groups. Regardless of the mechanistic details, this exergonic ketone−hydride insertion is too facile to be the turnover-limiting step of catalytic hydrogenations involving **5**/**6**, **8**/**9**, and **10** as intermediates. Further, the ratios of the product alkoxide diastereomers formed at low temperatures equaled within experimental error the ratios formed at room temperature, showing the diastereoselectivity of the insertion is only mildly sensitive to temperature changes.

Although the ketone groups in **2**, **3**, and **4** are activated toward reduction by the α-ester groups, they are rather sterically crowded by the *gem*-methyl groups and (for **4**) to some extent by the *tert*-butyl ester substituents. Noyori has proposed,[1a] and calculations substantiate,[17] that protonation or hydrogen bonding to the carbonyl oxygen of unfunctionalized and certain functionalized ketones is required for, or enhances the rate of, ketone−hydride insertion. That there is little kinetic impediment toward ketone−hydride insertion in this system shows that functionalized ketone−hydride insertion can be quite rapid in the absence of acid for hydride−catalyst systems with a vacant coordination site cis to the hydride.

Isolated Ruthenium−Alkoxide Complexes as Probable Catalytic Intermediates. The rates of stoichiometric hydrogenolysis of the ruthenium−alkoxide bonds in $\mathbf{5}_{(\mathrm{RuOC}D-)}$, $\mathbf{6}_{(\mathrm{RuOC}D-)}$, $\mathbf{8}_{(\mathrm{RuOC}D-)}$, $\mathbf{9}_{(\mathrm{RuOC}D-)}$, and $\mathbf{10}_{(\mathrm{RuOC}D-)}$ were much lower than the rates of ketone−hydride insertion. The ketone−hydride insertions were complete on mixing at room temperature, and they even occurred at −30 °C. The stoichiometric hydrogenolyses only occurred at significant rates under the conditions of the catalytic hydrogenation (50 °C and 50 atm of H_2). The stoichiometric hydrogenolyses were complete after 1 h under these conditions. This rate is comparable to the turnover frequencies of the catalytic hydrogenations (∼1 turnover/h in THF or in MeOH).[18] Within the accuracy of these experiments, the rate of the stoichiometric hydrogenolysis is consistent with the turnover frequency of the catalytic hydrogenation. These rate experiments thus cannot rule out the diastereomeric alkoxides as catalytic intermediates.

The rate and structural data suggest that the diastereomeric catalyst−alkoxides are catalytic intermediates. If this suggestion is correct, the mechanism of the catalytic hydrogenation involves a rapid, exergonic ketone−hydride insertion followed by a significantly slower, turnover-limiting hydrogenolysis of the ruthenium−alkoxide bond. This proposed mechanism imposes two preliminary requirements on the system that should be fulfilled before the mechanism can be considered further. The first requirement is that the diastereomeric catalyst−alkoxides actually form under catalytic conditions. The second requirement, imposed by the relative rates of the exergonic insertion (fast) and the hydrogenolysis (slow), is that the alkoxides are the predominant ruthenium-containing species in solution during catalysis. To investigate these issues, the catalytic hydrogenation of the di-*tert*-butyl ester **4** (50 °C and 50 atm of H_2) was interrupted by depressurization and cooling to room temperature after ∼4 turnovers. As predicted by the proposed mechanism, the catalyst−alkoxide diastereomer **10** was the sole detectable ruthenium-containing species present in the reaction mixture after the hydrogenation was interrupted. Assuming that **10** formed during the catalytic reaction, and not as some consequence of depressurization, this observation indicates the diastereomeric alkoxides are the major ruthenium species in solution during the catalytic hydrogenation.

The stoichiometric hydrogenolysis of $\mathbf{5}_{(\mathrm{RuOC}D-)}$, $\mathbf{6}_{(\mathrm{RuOC}D-)}$, $\mathbf{8}_{(\mathrm{RuOC}D-)}$, $\mathbf{9}_{(\mathrm{RuOC}D-)}$, and $\mathbf{10}_{(\mathrm{RuOC}D-)}$ were carried out in MeOH and THF under the conditions of the catalytic hydrogenation (under 50 atm of H_2 at 50 °C) to determine if ketone−hydride insertion was reversible on the time scale of the hydrogenolysis. If the reverse of ketone−deuteride insertion (a net β-deuteride

(15) The analysis of the variable-temperature ROESY NMR data for the *tert*-butyl complex **10** also corroborated the structure. While the complex **5** was complicated by overlap with signals from **6**, the resulting patterns also correspond to those observed with the complexes of **8** and **10**.

(16) For references on ketone/aldehyde metal hydride insertions see: (a) Nietlispach, D.; Veghini, D.; Berke, H. *Helv. Chim. Acta* **1994**, *77*, 2197. (b) Portnoy, M.; Milstein, D. *Organometallics* **1994**, *13*, 600. (c) Vanderzeijden, A. A. H.; Bosch, H. W.; Berke, H. *Organometallics* **1992**, *11*, 2051. (d) Vanderzeijden, A. A. H.; Berke, H. *Helv. Chim. Acta* **1992**, *75*, 513. (e) Esteruelas, M. A.; Valero, C.; Oro, L. A.; Meyer, U.; Werner, H. *Inorg. Chem.* **1991**, *30*, 1159. (f) Rakowski, M. C.; Muetterties, E. L. *J. Am. Chem. Soc.* **1977**, *99*, 739 and references sited therein.

(17) (a) Yamakawa, M.; Ito, H.; Noyori, R. *J. Am. Chem. Soc.* **2000**, *122*, 1466. (b) Alonso, D. A.; Brandt, P.; Nordin, S. J. M.; Andersson, P. G. *J. Am. Chem. Soc.* **1999**, *121*, 9580.

(18) The turnover frequencies were determined by interrupting catalytic hydrogenations of **2**, **3**, and **4** at time *t* and dividing the number of turnovers by *t*.

Scheme 2. Sequence of Steps for H−D Exchange at Alkoxide Carbon of Diastereomeric Ruthenium−Alkoxides

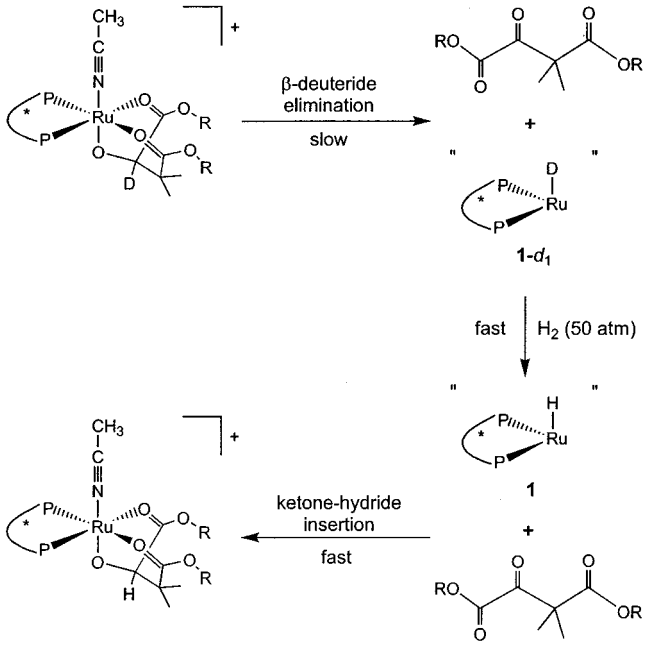

elmination) occurs at a rate faster than hydrogenolysis of the ruthenium−alkoxide bond, H−D exchange will occur at the alkoxide carbon via the following sequence of steps. β-Deuteride elmination within the diastereomeric catalyst−alkoxides followed by substrate dissociation will form the ketone (**2**, **3**, or **4**, respectively) and the deuterium-labeled catalyst (**1**-d_1) (Scheme 2). We have shown previously that the active catalyst **1** rapidly undergoes H−D exchange under ∼1 atm of D_2 even at low temperatures.[6b] Any **1**-d_1 generated by β-deuteride elmination within the diastereomeric catalyst−alkoxides will undergo H−D exchange immediately upon formation under catalytic conditions (50 atm of H_2, 50 °C) to generate the unlabeled catalyst **1**. Ketone−hydride insertion between **1** and the substrate followed by hydrogenolysis will then form the unlabeled product alcohol. The amount of H−D exchange at the alkoxide carbon in the product ($(MeO_2C)CD(OH)C(Me)_2(CO_2Me)$) of stoichiometric hydrogenolysis of $\mathbf{5}_{(RuOCD-)}$ and $\mathbf{6}_{(RuOCD-)}$ under catalytic conditions (50 atm of H_2, 50 °C) was ∼30% in MeOH and ∼40% in THF. Only 15% H−D exchange was observed in MeOH and 20% in THF during the stoichiometric hydrogenolysis of $\mathbf{8}_{(RuOCD-)}$ and $\mathbf{9}_{(RuOCD-)}$. The stoichiometric hydrogenolysis of $\mathbf{10}_{(RuOCD-)}$ resulted in only 10% H−D exchange in MeOH and 20% exchange in THF. These experiments prove that ketone−hydride insertion is only partially reversible (in one case only 10%) on the time scale of hydrogenolysis of the ruthenium−alkoxide bond under the conditions of catalytic hydrogenation. In other words, the rate of hydrogenolysis of the ruthenium−alkoxide bond is faster than the rate the catalyst alkoxides revert to catalyst and free ketone under catalysis conditions. The hydrogenolysis *does not* proceed via a rapid (fully established) preequilibrium between the diastereomeric alkoxides (traditionally called Curtin−Hammett conditions) under catalytic conditions.

The structure, rate, interruption, and deuterium exchange data support the proposal that the catalytic hydrogenation proceeds via a rapid ketone−hydride insertion followed by a slow hydrogenolysis of the ruthenium alkoxide bond. The data further indicate that the rate of hydrogenolysis is faster than the rate the alkoxides revert to free catalyst and ketone under conditions of the catalytic hydrogenation. If this mechanistic proposal is correct, rapid preequilibrium between the diastereomeric alkoxides will not occur during the catalytic hydrogenation, and the ratio of the diastereomeric alkoxides will reflect the ratio of alcohol product enantiomers. In other words, the enantioselectivity of such a mechanism is weighted more toward formation of the diastereomeric alkoxides and less toward hydrogenolysis of the ruthenium−alkoxide bond. We found that the ratio of alcohol product enantiomers obtained from the catalytic hydrogenation of **2** in THF (79.5 (*R*):20.5 (*S*) (the same ratio was obtained in MeOH)) was similar to the ratios of the catalyst−alkoxide diastereomers formed by the stoichiometric ketone−hydride insertions between **2** and **1** carried out at room temperature under ∼1 atm of dihydrogen (79 (*R*):21 (*S*) in THF (75 (*R*):25 (*S*) in MeOH)). Such similarities between the alcohol catalysis product enantiomer ratio and the catalyst−alkoxide diastereomer ratio were also obtained by using the diisopropyl ketone substrate **3** (catalysis product enantiomer ratio, 83 (*R*):17 (*S*); stoichiometric diastereomer ratio, 90 (*R*):10 (*S*)) and the di-*tert*-butyl ketone substrate **4** (catalysis product enantiomer ratio, 90 (*R*):10 (*S*); stoichiometric diastereomer ratio, ∼100 (*R*): ∼0 (*S*)) in THF.[19] These similarities in product ratios between the stoichiometric insertions and the catalytic hydrogenations imply that the stoichiometric insertions carried out under ∼1 atm of dihydrogen represent the insertions that proceed under catalytic conditions (50 atm of H_2 and 50 °C). This implication is supported by two observations. First, the de of the diastereomeric catalyst−alkoxide **10** isolated from the interrupted catalytic hydrogenation of **4** (∼100%) was the same as the de's of **10** obtained from the room temperature and low-temperature stoichiometric insertions (∼100%). Second, the de of the insertion reaction is only mildly sensitive to temperature changes (vide supra). These stoichiometric insertion reactions therefore support the prediction by the proposed mechanism that the enantioselection of the catalytic hydrogenation is weighted toward the ketone−hydride insertion step. We point out, however, that the de of the diastereomeric alkoxide **10** was ∼100%, while the ee's of the catalytic hydrogenations were from 80 to 84%, showing the hydrogenolysis also contributes to the enantioselection by such a catalytic cycle, but to a lesser extent than the ketone−hydride insertion.

Finally, and as expected if the diastereomeric alkoxides were true catalytic intermediates, the ee's of the alcohols obtained from the stoichiometric hydrogenolyses carried out under catalytic conditions (50 atm of H_2, 50 °C) were quite close to the ee's obtained from the catalytic hydrogenation (% ee from hydrogenolysis (ee from catalytic hydrogenation): $\mathbf{5}_{(RuOCD-)}$/$\mathbf{6}_{(RuOCD-)}$, 60 (59) in MeOH, 58 (59) in THF; $\mathbf{8}_{(RuOCD-)}$/$\mathbf{9}_{(RuOCD-)}$, 70 (68) in MeOH, 69 (66) in THF; $\mathbf{10}_{(RuOCD-)}$, 84 (82) in MeOH, 84 (80) in THF). The slight differences between the stoichiometric and catalytic ee's likely arise from experimental factors such as reaction occurring during warm-up of the pressure reactor during the stoichiometric hydrogenolysis and from isotope effects (the ee for the stoichiometric hydrogenolysis of **10** in THF was 82% versus 84% for $\mathbf{10}_{(RuOCD-)}$). These experiments show that the product ee's from stoichiometric hydrogenolysis of the mixture of diastereomeric alkoxides

(19) These stoichiometric reactions were not carried out in MeOH.

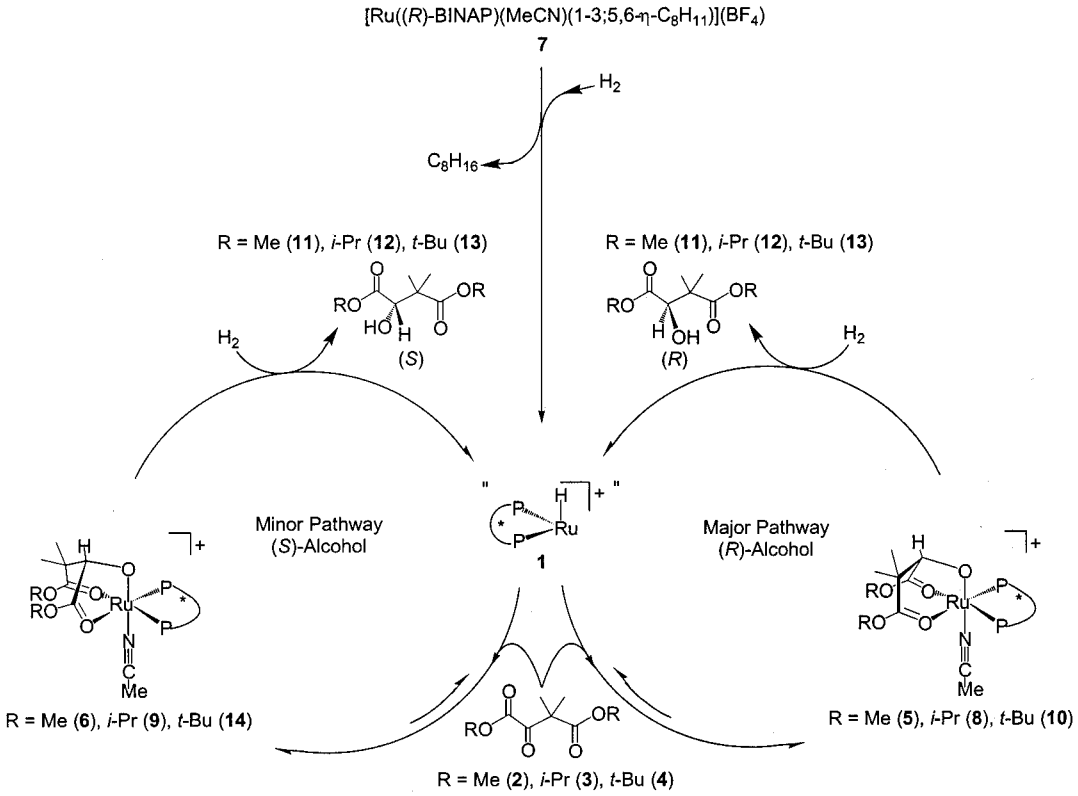

Figure 5. Proposed catalytic cycle. The active catalyst **1** proceeds through a major and minor pathway where the major pathway also corresponds to the major diastereomeric catalyst−alkoxide species observed in solution (**5**, **8**, and **10**).

formed at room temperature under ∼1 atm of dihydrogen is quite close to the product ee's of the catalytic hydrogenation. This evidence, along with the proof from the deuterium exchange experiments that the rate of hydrogenolysis is faster than the rate the diastereomeric alkoxides revert to free catalyst and ketone (vide supra), is strong indication that the diastereomeric alkoxides are actual catalytic intermediates. In other words, the mixture of diastereomeric alkoxides formed at room temperature reacts with dihydrogen to form alcohol product in nearly the same ee as the catalytic hydrogenation at a rate faster than they could invert absolute configuration by reversion to free catalyst and ketone. We point out, however, that high-pressure kinetics and NMR studies are required to rigorously prove this conclusion.

Proposed Mechanistic Pathway and Origins of Enantioselection. The rate of hydrogenolysis of the ruthenium−alkoxide bonds in the isolated diastereomeric alkoxides was consistent with the catalytic turnover frequency under the same reaction conditions. The ratio of diastereomeric alkoxides formed by stoichiometric ketone−hydride insertion is similar to the ratio of enantiomers formed by the catalytic hydrogenation. The stoichiometric hydrogenolysis does not proceed by a rapid (fully established) preequilibrium between the diastereomeric alkoxides, and the stoichiometric ee of the product alcohols is quite close to the catalytic ee. Taken together, these results are strong evidence that the diastereomeric catalyst−alkoxides formed by ketone−hydride insertion reactions between the active catalyst **1** and the ketone substrates **2**, **3**, and **4** are catalytic intermediates. Figure 5 shows the mechanism for the catalytic hydrogenation we propose based on the mechanistic and structural evidence presented in this paper. Hydrogenation of the catalyst precursor (**7**) forms cyclooctane and the active catalyst species **1**. The ketone substrate (**2**, **3**, or **4**) then undergoes fast, exergonic insertion into the Ru−H bond to yield the major and minor diastereomeric catalyst−alkoxide intermediates (**5** and **6**; **8** and **9**; and **10** from ketones **2**, **3**, and **4**, respectively). This insertion is only partially reversible on the time scale of hydrogenation, and it contributes greatly to the enantioselection by the catalytic cycle. In the subsequent steps, the ruthenium−alkoxide bond is irreversibly cleaved, likely by the addition of dihydrogen, releasing the chiral alcohol product and reforming the active catalyst species **1** to complete the catalytic cycle. As the catalyst−alkoxides are 18-electron species, it is proposed that either desolvation of the MeCN ligand or dissociation of a coordinated ester occurs prior to addition of H_2 and subsequent reductive elimination of the alcohol products.

The weight of evidence that the diastereomeric alkoxides are catalytic intermediates warrants consideration of possible links between their structures and the enantioselection by the catalytic hydrogenation. As stated previously, that the rate of hydrogenolysis is faster than the rate of reversion to free catalyst and ketone, and that the ratio of diastereomeric alkoxides is similar to the ratio of product alcohol enantiomers is strong evidence that the catalytic enantioselection is weighted toward the steps prior to the hydrogenolysis. Both the ratio of product enantiomers from the catalytic hydrogenation and the ratio of diastereomeric alkoxides increase when the steric bulk of the ester groups is increased. This is evidence that there is a relationship between the relative energies of the diastereomeric alkoxides and the enantioselection by the catalytic cycle. By assuming the minor diastereomer has the same broad structural features (alkoxide group and MeCN are both cis to both phosphorus centers, and both ester groups coordinated) the steric origins of

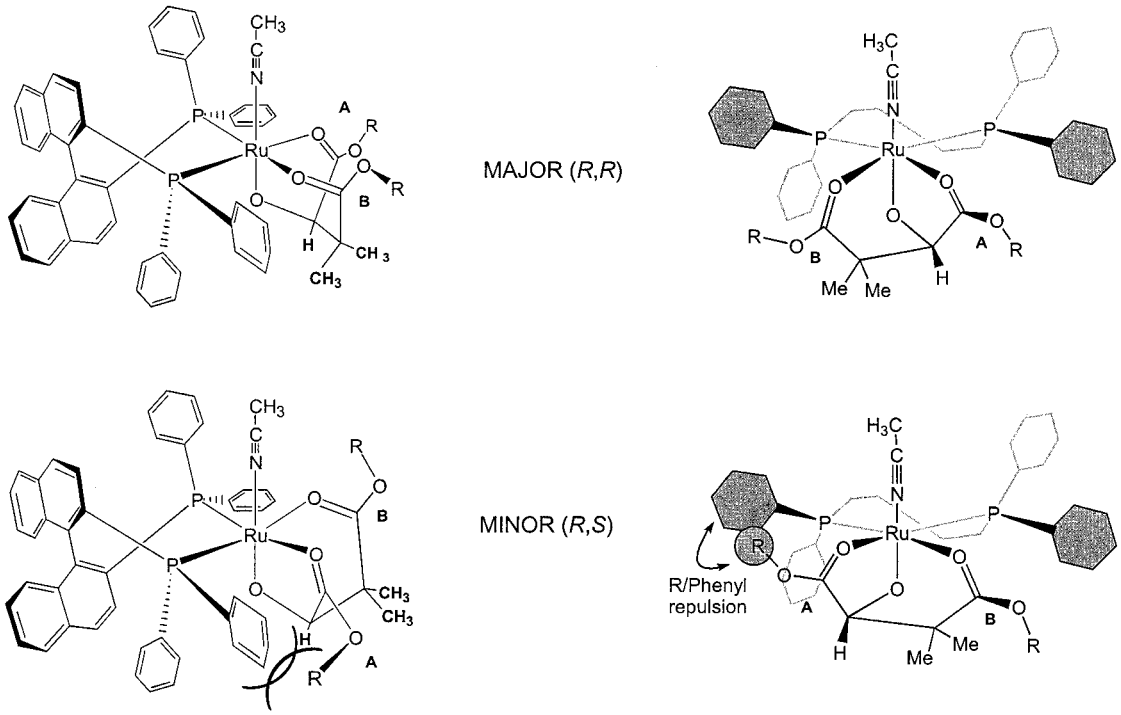

Figure 6. Possible steric influence on enantioselection. Increasing ester group size increases the severity of steric interactions of the minor diastereomer, and increases the overall enantioselection, the *tert*-butyl ester giving the greatest enantioselection. Note rotation about the phosphorus−phenyl bonds is rapid at room temperature.

the energy difference between the diastereomers becomes apparent. Figure 6 illustrates this steric interaction.

Inspection of molecular models reveals no significant steric repulsions in the major diastereomer. The minor diastereomer, however, contains a strongly repulsive steric interaction between the ester alkoxy group A (α-ester to ketone carbonyl) and P_2−Ph_{eq}. The steric crowding between these groups increases as does the size of the ester alkoxy groups, and we propose that it is this interaction that is responsible for the enantioselection by the catalytic cycle.

Conclusions

This work presents the first *complete and unambiguous* structure determination of a diastereomeric substrate−catalyst adduct in an enantioselective ketone hydrogenation. It also provides the first direct experimental information on the reaction dynamics of how such diastereomers form, on how they react, and on the steric forces within these probable catalytic intermediates. In these systems, ketone−hydride insertion is rapid and exergonic, and it may proceed without prior formation of an η^2-π-ketone−catalyst complex. Further, the rate of hydrogenolysis is higher than the rate of reversion to catalyst and ketone. The structural and mechanistic evidence we obtained strongly supports that these catalytic hydrogenations operate by the mechanism shown in Figure 5. In this mechanism, and unlike hydrogenations of MAC and related olefin substrates catalyzed by [Rh(chiral bisphosphine)$(sol)_2$]$^+$, the diastereomeric catalyst−substrate intermediate present in the highest concentration leads to the major product enantiomer.[20] The net enantioselectivity of the catalytic cycle is partitioned between the partially reversible ketone−hydride insertion and hydrogenolysis of the ruthenium−alkoxide bond, but it is weighted toward the ketone−hydride insertion. As is the case with any mechanism study, caution must be exercised when extending these results to other systems.

Experimental Section

Materials and Methods. All operations were performed under an argon atmosphere with standard Schlenk techniques. The solvents were dried and distilled under an argon atmosphere by standard methods before use.[21] The argon gas (Praxair, 99.998%) was passed through a drying train containing 3 Å molecular sieves and P_4O_{10} before use. Trace quantities of oxygen were removed from the dihydrogen gas (Praxair, 99.99%) by passage through an Alltech Oxy-Trap. All commercial reagents (Aldrich or Fluka) were recrystallized or distilled under an argon atmosphere before use. [Ru((*R*)-BINAP)(MeCN)(1-3:5,6-η-C_8H_{11})](BF$_4$) (**7**),[5a] dimethyl oxaloacetate,[22] and di-*tert*-butyl oxaloacetate[22] were prepared using established procedures.

Unless stated otherwise, all ^{1}H, ^{13}C, and ^{31}P NMR spectra were measured with Bruker AM-400 or AM-500 spectrometers. ^{1}H and ^{13}C NMR chemical shifts are reported in parts per million (δ) relative to TMS with the solvent as an internal reference. ^{31}P NMR chemical shifts are reported in parts per million (δ) relative to an 85% H_3PO_4 external reference. All ^{13}C and ^{31}P NMR are ^{1}H decoupled unless stated otherwise. Mass spectra were measured with a Kratos MS50 spectrometer. Microanalyses were performed at the University of Alberta Microanalysis Laboratory. Optical rotations were measured with a Perkin-Elmer 241 polarimeter at 589 nm with 1.0 dm cells. Specific rotations, $[\alpha]_D$, are reported in degrees per decimeter at 25 °C, and the concentration (c) is given in grams per 100 mL.

Diisopropyl Acetylenedicarboxylate. To a 100 mL flask was transferred acetylene dicarboxylic acid (20.0242 g, 1.756×10^{-1} mol),

(20) As stated previously, a high-pressure kinetics investigation should support this mechanistic scheme. We note that the alkoxides cannot be mere catalytic sinks because they react with little reversible formation at approximately the same rate as the turnover frequency.

(21) Casey, M.; Leonard, J.; Lygo, B.; Procter, G. *Advanced Practical Organic Chemistry*; Chapman & Hall: London, 1990; p 28.
(22) Sucrow, W.; Grosz, K. P. *Synth. Commun.* **1979**, *9*, 603.

concentrated H_2SO_4 (2.5 mL), and 2-propanol (150 mL). The solution was stirred and heated to reflux (80 °C) for 5 h, after which it was cooled to room temperature and then concentrated under reduced pressure. The remaining clear−colorless liquid was taken up in Et_2O (100 mL) and sequentially washed with a 2 N solution of NaOH until the aqueous layer was basic (2 × 20 mL) and with distilled H_2O (4 × 25 mL). The organic layer was dried over $MgSO_4$ for 24 h, filtered, and washed with Et_2O (3 × 100 mL), and the solvent was removed under reduced pressure yielding the clear−colorless liquid product (30.2 g, 86.8%). The product was used without further purification. ^{1}H NMR (400.1 MHz, CD_2Cl_2, 25 °C): δ 1.28 (d, 12H, $^3J_{H-H}$ = 6.5 Hz, RC≡CR, R = $CO_2C(CH_3)_2$(H)), 5.12 (quint, 2H, $^3J_{H-H}$ = 6.5 Hz, RC≡CR, R = $CO_2C(CH_3)_2$(H)). ^{13}C NMR (100.6 MHz, CD_2Cl_2, 25 °C): δ 21.58 (4C, RC≡CR, R = $CO_2C(CH_3)_2$(H)), 71.34 (2C, RC≡CR, R = $CO_2C(CH_3)_2$(H)), 74.68 (2C, RC≡CR, R = $CO_2C(CH_3)_2$(H)), 151.45 (2C, RC≡CR, R = $CO_2C(CH_3)_2$(H)).

Dimethyl 3,3-Dimethyloxaloacetate (2). To a dry 100 mL flask was transferred potassium carbonate (1.76 g, 12.8 mmol). The flask was flushed with dry argon gas for 20 min and then charged with dimethyl oxaloacetate (1.02 g, 6.38 mmol) and acetone (30 mL, distilled). A condenser was added to the flask and the system was kept under an argon atmosphere. The solution was stirred for 5 min then methyl iodide (2.4 mL, 38.3 mmol) was added down the condenser, and the mixture was heated and stirred under reflux for 20 h. The solution was then cooled and the solvent removed under reduced pressure. The solid residue was washed with CH_2Cl_2 (20 mL) and passed through a column of alumina (10 cm long, 1 cm diameter). The column was further washed with CH_2Cl_2 (20 mL) and the solvent was removed under reduced pressure to yield a clear pale yellow liquid (0.97 g, 80.8% yield). ^{1}H NMR (400 MHz, CD_2Cl_2, 25 °C): δ 1.39 (s, 6H, $C(CH_3)_2$), 3.67 (s, 3H, CO_2CH_3), 3.82 (s, 3H, CO_2CH_3). ^{13}C NMR (400 MHz, CD_2Cl_2, 25 °C): δ 21.94 (2C, $C(CH_3)_2$), 52.76 (1C, CO_2CH_3), 52.92 (1C, $C(CH_3)_2$), 53.33 (1C, CO_2CH_3), 160.94 (1C, CO_2CH_3), 173.24 (1C, CO_2CH_3), 191.77 (1C, $C(O)CO_2CH_3$). CI-MS (pos) *m*/*z* 206.1 ($(M + NH_4)^+$, exact mass calcd for $C_8H_{12}O_5 + NH_4^+$ = 206.2). Anal. Calcd for $C_8H_{12}O_5$: C, 51.06; H, 6.43. Found: C, 50.89; H, 6.58.

Diisopropyl 3,3-Dimethyloxaloacetate (3). The synthesis was performed with a similar procedure as in the synthesis of dimethyl-3,3-dimethyloxaloacetate. ^{1}H NMR (400 MHz, $CDCl_3$, 25 °C): δ 1.19 (d, 6H, $^3J_{H-H}$ = 6.5 Hz, $CO_2C(CH_3)_2$(H)), 1.33 (d, 6H, $^3J_{H-H}$ = 6.5 Hz, $CO_2C(CH_3)_2$(H)), 1.42 (s, 6H, $C(CH_3)_2$), 5.03 (quint, 1H, $^3J_{H-H}$ = 6.5 Hz, $CO_2C(CH_3)_2$(H)), 5.11 (quint, 1H, $^3J_{H-H}$ = 6.5 Hz, $CO_2C(CH_3)_2$(H)).

Di-*tert*-butyl 3,3-Dimethyloxaloacetate (4). The synthesis was performed with a similar procedure as in the synthesis of dimethyl 3,3-dimethyloxaloacetate. ^{1}H NMR (400 MHz, $CDCl_3$, 25 °C): δ 1.39 (s, 6H, $C(CH_3)_2$), 1.43 (s, 9H, $CO_2C(CH_3)_3$), 1.55 (s, 9H, $CO_2C(CH_3)_3$). FT-IR (CH_2Cl_2, 22 °C): 1744 cm^{-1} (shoulder, $\nu_{C=O}$), 1725 cm^{-1} (s, $\nu_{C=O}$).

2,2-Dimethylbutan-1,3,4-triol. $LiAlH_4$ (0.122 g, 3.21 × 10^{-3} mol) was transferred to a three-necked flask that had an addition funnel and septa. To the addition funnel were transferred the hydrogenated product **13** (90.0 mg, 3.28 × 10^{-4} mol) and Et_2O (5 mL). To the flask was transferred Et_2O (15 mL) via cannula. The system was flushed with argon gas for 10 min and then left under an argon atmosphere. The flask was cooled to −5 °C and, after 5 min, the alcohol Et_2O solution was added dropwise over 10 min. The addition funnel was rinsed with Et_2O and the solution was allowed to react for 1.5 h at ambient-temperature. The flask was then cooled back to −5 °C and distilled water (125 μL) was added slowly over 30 s. Next, 0.1 N HCl (125 μL) and distilled water (375 μL) were added dropwise in succession. The solution was allowed to react for 30 min, then it was filtered and the solid washed with Et_2O (4 × 10 mL). The solvent was then removed under reduced pressure yielding the clear−colorless liquid product (38.2 mg, 86.8% yield). A similar procedure was utilized for the reduction of **12** (85.5% yield). ^{1}H and ^{13}C NMR correspond to literature data.[23]

[Ru((*R*)-BINAP)(MeCN)(OC(H)(CO_2CH_3)(C(CH_3)$_2$(CO_2CH_3)))]-(BF_4) (5/6). To a 20 mL solvent Schlenk was transferred **7** (100.5 mg, 1.05 × 10^{-4} mol). The flask was placed under vacuum and refilled with argon gas (×3) to remove all traces of oxygen. To a sidearm flask was transferred **2** (21.7 mg, 1.15 × 10^{-4} mol) in the glovebox. Next, solvent (1.5 mL; acetone, THF, or methanol) was added to the flask via gastight syringe and the solution was transferred to the solvent Schlenk via cannula. The flask was rinsed with solvent (8.5 mL) and transferred to the solvent Schlenk. The tube was flushed with dihydrogen gas for 2 min and then pressurized to 20 psig. The tube was shaken vigorously until all of the catalyst precursor was in solution, and for a further 5 min to ensure complete reaction. The tube was then depressurized to atmospheric pressure under argon gas, the solution transferred to a sidearm flask, and the solvent removed under reduced pressure. The solid residue was redissolved in THF (2.0 mL) and precipitated with pentane (25 mL). The solution was filtered and the solid washed with pentane (3 × 5 mL) and dried under high vacuum for 2 h (96.3 mg, 88.7% yield). The ratio of products observed by ^{31}P NMR analysis when synthesized was 79:21 in THF and 75:25 in methanol. To obtain ^{15}N-enriched complexes, the compounds were dissolved in acetone and excess ^{15}NCMe was added. The solution was stirred for 2 h and ^{31}P NMR analysis indicated >95% exchange of ^{14}NCMe with ^{15}NCMe had occurred. FT-IR (CH_2Cl_2, 22 °C): 1608 cm^{-1} (w, $\nu_{C=O}$), 1636 cm^{-1} (s, $\nu_{C=O}$). ESI-MS (pos) *m*/*z* 954.1 $(M)^+$, exact mass calcd for $C_{54}H_{48}O_5NP_2Ru^+$, 954.2. Anal. Calcd for $C_{54}H_{48}O_5NP_2RuBF_4$: C, 62.32; H, 4.65; N, 1.35. Found: C, 61.97; H, 4.44; N, 1.37. **5** (absolute configuration (*R*)): ^{1}H NMR (400 MHz, acetone-d_6, 25 °C): δ 0.94 (s, 3H, $C(CH_3)_2$), 1.03 (s, 3H, $C(CH_3)_2$), 1.93 (s, 3H, CH_3CN), 3.41 (s, 3H, α-$C(O)OCH_3$), 3.62 (s, 3H, β-$C(O)OCH_3$), 3.84 (br s, 1H, Ru−O−C*H*, overlapped with minor), 6.45−7.95 (m, 32H, BINAP, overlapped with minor). ^{13}C NMR (400 MHz, acetone-d_6, 25 °C): δ 4.09 (1C, CH_3CN), 21.04 (1C, $C(CH_3)_2$), 25.35 (1C, $C(CH_3)_2$), 46.98 (1C, $C(CH_3)_2$), 55.0 (1C, CO_2CH_3), 55.1 (1C, CO_2CH_3), 86.7 (1C, Ru−O−*C*H, overlapped with minor), 126.8 (1C, CH_3CN), 127−142.5 (BINAP, overlapped with minor), 183.5 (1C, β-CO_2CH_3), 190.2 (1C, α-CO_2CH_3, overlapped with minor). ^{31}P NMR (400 MHz, acetone-d_6, 25 °C): δ 58.9 (d, 1P, $^2J_{P-P}$ = 45.5 Hz), 62.3 (d, 1P, $^2J_{P-P}$ = 45.5 Hz). ^{31}P NMR (400 MHz, acetone-d_6, 25 °C) of ^{15}NCMe enriched compound: δ 58.9 (dd, 1P, $^2J_{P-P}$ = 45.0 Hz, $^2J_{P-N}$ = 2.8 Hz), 62.3 (dd, 1P, $^2J_{P-P}$ = 45.0 Hz, $^2J_{P-N}$ = 2.8 Hz).

6 (absolute configuration (*S*)): ^{1}H NMR (400 MHz, acetone-d_6, 25 °C): δ 1.12 (br s, 3H, $C(CH_3)_2$), 1.19 (br s, 3H, $C(CH_3)_2$), 1.89 (s, 3H, CH_3CN), 3.37 (br s, 3H, α-$C(O)OCH_3$), 3.52 (br s, 3H, β-$C(O)OCH_3$), 3.84 (br s, 1H, Ru−O−C*H*, overlapped with major), 6.45−7.95 (m, 32H, BINAP, overlapped with major). ^{13}C NMR (400 MHz, acetone-d_6, 25 °C): δ 4.3 (1C, CH_3CN), 22.0 (1C, $C(CH_3)_2$), 23.2 (1C, $C(CH_3)_2$), 49.2 (1C, $C(CH_3)_2$), 53.1 (1C, CO_2CH_3), 55.0 (1C, CO_2CH_3), 86.7 (1C, Ru−O−*C*H, overlapped with major), 126.8 (1C, CH_3CN, overlapped with major), 127−142.5 (BINAP, overlapped with major), 190.5 (1C, β-CO_2CH_3), 191.2 (1C, α-CO_2CH_3, overlapped with major). ^{31}P NMR (400 MHz, acetone-d_6, 25 °C): δ 57.4 (br d, 1P, $^2J_{P-P}$ = 45.0 Hz), 63.7 (br d, 1P, $^2J_{P-P}$ = 45.0 Hz). ^{31}P NMR (400 MHz, acetone-d_6, 25 °C) of ^{15}NCMe enriched compound: δ 57.4 (dd, 1P, $^2J_{P-P}$ = 45.5 Hz, $^2J_{P-N}$ = 2.9 Hz), 63.7 (dd, 1P, $^2J_{P-P}$ = 45.5 Hz, $^2J_{P-N}$ = 2.9 Hz).

[Ru((*R*)-BINAP)(MeCN)(OC(H)($CO_2CH(CH_3)_2$)(C(CH_3)$_2$($CO_2CH(CH_3)_2$))][BF_4] (8/9). (**8**/**9**) was synthesized in a similar manner as (**5**/**6**) in THF. FT-IR (CH_2Cl_2, 22 °C): 1610 cm^{-1} (w, $\nu_{C=O}$), 1638 cm^{-1} (s, $\nu_{C=O}$). ESI-MS (pos) *m*/*z* 1010.2 $(M)^+$, exact mass calcd for $C_{58}H_{56}O_5NP_2Ru^+$, 1010.268. Anal. Calcd for $C_{58}H_{56}O_5NP_2RuBF_4$: C, 63.51; H, 5.15; N, 1.28. Found: C, 63.15; H, 5.32; N, 1.41. **8** (absolute configuration (*R*)): ^{1}H NMR (400 MHz, THF-d_8, 25 °C): δ 0.76 (d, 3H, $^3J_{H-H}$ = 5.5 Hz, α-$CO_2(CH(CH_3)_2)$), 0.80 (s, 3H, $C(CH_3)_2$), 0.98

(23) Matsuo, T.; Mori, K.; Matsui, M. *Tetrahedron Lett.* **1976**, *23*, 1979.

(s, 3H, C(CH_3)$_2$), 1.09 (d, 3H, $^3J_{H-H}$ = 5.5 Hz, β-CO$_2$(CH(CH_3)$_2$)), 1.15 (d, 3H, $^3J_{H-H}$ = 5.5 Hz, α-CO$_2$(CH(CH_3)$_2$)), 1.23 (d, 3H, $^3J_{H-H}$ = 5.5 Hz, β-CO$_2$(CH(CH_3)$_2$)), 1.89 (s, 3H, NCCH_3), 3.82 (s, 1H, Ru−O−C*H*), 4.76 (br quint, 1H, $^3J_{H-H}$ = 5.5 Hz, α-CO$_2$(C*H*(CH$_3$)$_2$)), 5.42 (br quint, 1H, $^3J_{H-H}$ = 5.5 Hz, β-CO$_2$(C*H*(CH$_3$)$_2$)), 6.40−8.02 (m, 32H, BINAP). ^{13}C NMR (400 MHz, THF-d_8, 25 °C): δ 3.9 (1C, *C*H$_3$CN), 20−21 (3C, CH(*C*H$_3$)$_2$, 2 from α-ester group and 1 from β-ester group), 25.0 (1C, CH(*C*H$_3$)$_2$, from β-ester group), 46.0 (1C, *C*(CH$_3$)$_2$), 72.0 (1C, β-CO$_2$(*C*H(CH$_3$)$_2$)), 73.0 (1C, α-CO$_2$(*C*H(CH$_3$)$_2$)), 87.0 (1C, Ru−O−*C*H), 124−142 (46C, BINAP carbons), 182 (1C, β-*C*O$_2$(CH(CH$_3$)$_2$)), 190 (1C, α-*C*O$_2$(CH(CH$_3$)$_2$)). ^{31}P NMR (400 MHz, THF-d_8, 25 °C): δ 56.0 (d, 1P, $^2J_{P-P}$ = 47.0 Hz, P$_1$ of minor complex), 60.4 (d, 1P, $^2J_{P-P}$ = 45.0 Hz, P$_1$ of major complex), 64.1 (d, 1P, $^2J_{P-P}$ = 45.0 Hz, P$_2$ of major complex), 66.4 (d, 1P, $^2J_{P-P}$ = 47.0 Hz, P$_2$ of minor complex). ^{31}P NMR (400 MHz, acetone-d_6, 25 °C) of ^{15}NCMe enriched compound: δ 56.0 (dd, 1P, $^2J_{P-P}$ = 47.0 Hz, $^2J_{P-N}$ = 3.0 Hz, P$_1$ of minor complex), 60.4 (dd, 1P, $^2J_{P-P}$ = 45.0 Hz, $^2J_{P-N}$ = 2.7 Hz, P$_1$ of major complex), 64.1 (dd, 1P, $^2J_{P-P}$ = 45.0 Hz, $^2J_{P-N}$ = 2.7 Hz, P$_2$ of major complex), 66.4 (dd, 1P, $^2J_{P-P}$ = 47.0 Hz, $^2J_{P-N}$ = 3.0 Hz, P$_2$ of minor complex).

[Ru((*R*)-BINAP)(MeCN)(OC(H)(CO$_2$C(CH$_3$)$_3$)(C(CH$_3$)$_2$(CO$_2$C-(CH$_3$)$_3$))](BF$_4$) (10). 10 was synthesized in the same manner as (**5**/**6**) in THF. FT-IR (CH$_2$Cl$_2$, 22 °C): 1608 cm^{-1} (w, $\nu_{C=O}$), 1644 cm^{-1} (s, $\nu_{C=O}$). ESI-MS (pos) *m*/*z* 1038.3 (M)$^+$, exact mass calcd for $C_{60}H_{60}O_5NP_2RuBF_4$, 1038.298. Anal. Calcd for $C_{60}H_{60}O_5NP_2RuBF_4$: C, 64.06; H, 5.38; N, 1.25. Found: C, 63.32; H, 5.44; N, 1.54. **10** (absolute configuration (*R*)): ^{1}H NMR (400 MHz, THF-d_8, 25 °C): δ 0.86 (s, 3H, C(CH_3)$_2$), 1.07 (s, 3H, C(CH_3)$_2$), 1.17 (s, 9H, α-CO$_2$C(CH_3)$_3$), 1.50 (s, 9H, β-CO$_2$C(CH_3)$_3$), 1.92 (s, 3H, CH_3CN), 3.98 (s, 1H, Ru−O−C*H*), 6.5−8.04 (m, 32H, BINAP). ^{13}C NMR (400 MHz, THF-d_8, 25 °C): δ 3.78 (1C, *C*H$_3$CN), 22.24 (1C, C(*C*H$_3$)$_2$), 24.97 (1C, C(*C*H$_3$)$_2$), 28.30 (3C, OC(*C*H$_3$)$_3$), 28.78 (3C, OC(*C*H$_3$)$_3$), 48.20 (1C, *C*(CH$_3$)$_2$), 87.32 (1C, O*C*(CH$_3$)$_3$), 88.23 (1C, O*C*(CH$_3$)$_3$), 89.48 (1C, Ru−O−*C*H), 126.5−142.6 (42C, aromatics, BINAP), 183.41 (1C, β-*C*O$_2$C-(CH$_3$)$_3$), 190.20 (α-*C* CO$_2$C(CH$_3$)$_3$). ^{31}P NMR (400 MHz, THF-d_8, 25 °C): δ 59.5 (d, 1P, P$_1$, $^2J_{P-P}$ = 45.5 Hz), 63.5 (d, 1P, P$_2$, $^2J_{P-P}$ = 45.5 Hz). ^{31}P NMR (400 MHz, acetone-d_6, 25 °C) of ^{15}NCMe enriched compound: δ 59.5 (dd, 1P, P$_1$, $^2J_{P-P}$ = 45.0 Hz, $^2J_{P-N}$ = 2.8 Hz), 63.5 (dd, 1P, P$_2$, $^2J_{P-P}$ = 45.0 Hz, $^2J_{P-N}$ = 2.8 Hz). For details on the assignment of BINAP signals refer to the Results and Discussion section.

Low-Temperature NMR Investigation of Catalyst and Substrate Interactions. Compound **7** (19.5 mg, 2.03 × 10^{-5} mol) was partially dissolved in THF-d_8 (0.6 mL) in an NMR tube under an argon atmosphere. At room temperature, the tube was flushed with dihydrogen gas, pressurized (1−2 atm), and shaken until a golden orange solution was generated (∼5 min). The dihydrogen atmosphere was replaced by argon and the resulting solution was analyzed by ^{1}H and ^{31}P NMR spectroscopy at −80 °C. NMR spectroscopic analysis indicated a mixture of two ruthenium−hydrido species ([Ru((*R*)-BINAP)(H)(THF-d_8)$_n$(MeCN)$_{3-n}$](BF$_4$) (n = 0−3, with n = 2 as major species (75%))) and cyclooctane were present. At −80 °C, **2** (4.0 mg, 1.15 × 10^{-4} mol) was injected into the NMR tube via gastight syringe. The tube was removed from the cooling bath, shaken for ∼15 s, and then immediately placed in a precooled (−80 °C) NMR probe. The ^{31}P NMR spectrum at −80 °C remained unchanged, as did the ^{1}H NMR spectrum except for the introduction of **2**. Upon warming the NMR probe, the ^{31}P and ^{1}H NMR remained unchanged until the temperature reached −30 °C. At −30 °C, the ^{31}P NMR slowly showed the signs of **5** and **6** peaks growing in and no other peaks were observed. Once warmed to ambient temperature, the ^{31}P NMR showed only the presence of **5** and **6** in the same ratio observed with the stoichiometric reaction at room temperature. ^{31}P (162.0 MHz, THF-d_8, −80 to −40 °C): δ 72.2 (d, $^2J_{P-P}$ = 42.5 Hz, A), 72.4 (d, $^2J_{P-P}$ = 49.5 Hz, B), 77.1 (d, $^2J_{P-P}$ = 43.5 Hz, A), 81.4 (d, $^2J_{P-P}$ = 49.5 Hz, B). Approximate percentages of hydrido species present: A (25%) and B (75%). ^{31}P (162.0 MHz, THF-d_8, −30 °C): δ 59.8 (d, 1P, $^2J_{P-P}$ = 45.5 Hz, **5**), 63.0 (d, 1P, $^2J_{P-P}$ = 45.5 Hz, **5**), 56.4 (br d, 1P, $^2J_{P-P}$ ∼ 45 Hz, **6**), 63.7 (br d, 1P, $^2J_{P-P}$ ∼ 45 Hz, **6**). Similar results were observed upon low-temperature investigation of both **3** and **4**. The only observable species upon warming were the alkoxide intermediates **8** and **9** for **3** (in the same ratio observed in stoichiometric reaction of **1** with the ketone at room temperature) and only **10** for **4**.

Typical Procedure for Hydrogenation. To a 25 mL sidearm flask was transferred **7** (10.0 mg, 1.04 × 10^{-5} mol) and 50 equiv of the corresponding ketone (**2**, **3**, or **4**; 5.21 × 10^{-4} mol) in a glovebox. Solvent (methanol or THF, 5.0 mL) was added to the sealed flask via gastight syringe. The flask was transferred to a pre-flushed, argon gas, stainless steel bomb. The bomb was flushed for a further 15 min with argon gas, then with dihydrogen gas for 10 min, and finally it was pressurized to 50 atm. Once stabilized, the bomb was placed in a 50 °C oil bath and reacted for 50 h. The bomb was then cooled to ambient temperature and depressurized, and the flask was placed under reduced pressure to remove the solvent. The residue was passed through a Florisil plug with Et$_2$O (∼10 mL) to remove the catalyst. The Et$_2$O was removed under reduced pressure and the clear−colorless liquid products were analyzed by ^{1}H NMR. The enantiomeric excesses were determined by either ^{1}H NMR, with added shift reagent (tris[3-(heptafluoropropylhydroxy-methylene)-(+)-camphorato]europium(III)) and its comparison to that of the racemic alcohol and added shift reagent (used for **11** and **12**),[24] or by chiral GC analysis (**13**).[25] The absolute configuration of the major enantiomeric product **11** was determined by comparison to the reported optical rotation of (*S*)-**11** ([α]$_D$ +33°, *c* 1.42, CHCl$_3$).[26] The absolute configuration of the major enantiomeric product for **12** and **13** was determined by reduction of the products with LiAlH$_4$ to the corresponding triol, 2,2-dimethylbutan-1,3,4-triol, and comparison to the reported optical rotation of (3*R*)-(−)-2,2-dimethylbutan-1,3,4-triol ([α]$_D$ −16°, *c* 1.06, EtOH).[23] ^{1}H NMR of **11** (400.1 MHz, CDCl$_3$, 25 °C): δ 1.12 (s, 3H, C(CH_3)$_2$), 1.21 (s, 3H, C(CH_3)$_2$), 3.23 (br d, 1H, $^3J_{H-H}$ ∼ 6 Hz, C(H)(O*H*)), 3.66 (s, 3H, OCH_3), 3.72 (s, 3H, OCH_3), 4.30 (br d, 1H, $^3J_{H-H}$ ∼ 6 Hz, C(*H*)(OH)). ^{1}H NMR of **12** (400.1 MHz, CDCl$_3$, 25 °C): δ 1.12 (s, 3H, C(CH_3)$_2$), 1.22 (s, 3H, C(CH_3)$_2$), 1.23 (d, 6H, $^3J_{H-H}$ = 6.5 Hz, CO$_2$C((CH_3)$_2$-(H))), 1.24 (d, 6H, $^3J_{H-H}$ = 6.5 Hz, CO$_2$C((CH_3)$_2$(H))), 3.19 (d, 1H, $^3J_{H-H}$ = 6.5 Hz, C(H)(O*H*)), 4.30 (d, 1H, C(*H*)(OH)), 4.99 (quint, 1H, $^3J_{H-H}$ = 6.5 Hz, CO$_2$C((CH$_3$)$_2$(*H*))), 5.08 (quint, 1H, $^3J_{H-H}$ = 6.5 Hz, CO$_2$C((CH$_3$)$_2$(*H*))). ^{1}H NMR of **13** (400.1 MHz, CDCl$_3$, 25 °C): δ 1.14 (s, 3H, C(CH_3)$_2$), 1.68 (s, 3H, C(CH_3)$_2$), 1.44 (s, 9H, CO$_2$C(CH_3)$_3$), 1.48 (s, 9H, CO$_2$C(CH_3)$_3$), 3.19 (d, 1H, C(H)(O*H*)), 4.17 (d, C(*H*)-(OH)).

Stoichiometric Hydrogenolysis of [Ru((*R*)-BINAP)(MeCN)(OC-(D)(CO$_2$R)(C(CH$_3$)$_2$(CO$_2$R))](BF$_4$) (5-d_1/6-d_1, 8-d_1/9-d_1, and 10-d_1). In the glovebox, the mixture of complexes **5**-d_1 and **6**-d_1 (105.0 mg, 1.01 × 10^{-4} mol) was transferred to a 100 mL sidearm. The flask was sealed and the solvent (MeOH or THF, 48.6 mL) added via gastight syringe. The sidearm was placed in a preflushed stainless steel bomb and the bomb was further flushed for 15 min with argon gas and with dihydrogen gas for 10 min, and finally pressurized to 50 atm. The bomb was allowed to react for 1 h (the time, on average, for a single turnover in the operating catalytic reaction) in a 50 °C oil bath. Once the bomb was depressurized, the flask was removed and bubbled with oxygen to destroy the catalyst. The flask was then placed under reduced pressure to remove the solvent. The residue was passed through a Florisil plug with Et$_2$O (5 mL) to remove the catalyst, the solvent removed under reduced pressure, and the product analyzed by NMR. ^{1}H NMR of THF

(24) **11**: The ratio of the methoxy signals (ca. δ 4.0) was used to determine the ee. The ratio of these peaks was 1:1 for racemic alcohol. **12**: The ratio of the backbone methyl signals (ca. δ 1.2 and 1.1) was used to determine the ee. The ratio of these peaks was 1:1 for racemic alcohol.

(25) Performed on a Beta Dex 120 column in acetone solution. Initial oven temperature was 120 °C for 45 min then it was increased at a rate of 10 °C/min to 200 °C. The enantiomers were eluted at ∼ 45 min for (*S*)-enantiomer and at ∼46 min for (*R*)-enantiomer.

(26) Seebach, D.; Wasmuth, D. *Helv. Chim. Acta* **1980**, *63*, 197.

reaction (400.1 MHz, $CDCl_3$, 25 °C): δ 4.3 (0.4 H as compared to 3H methoxy signals at ca. δ 3.8). The ee was determined to be 58% (*R*). ^{1}H NMR of MeOH reaction (400.1 MHz, $CDCl_3$, 25 °C): δ 4.3 (0.25 H as compared to 3H methoxy signals at ca. δ 3.8). The ee was determined to be 60% (*R*). The stoichiometric hydrogenations of the complexes **8**-d_1/**9**-d_1 and **10**-d_1 were performed in a similar manner. ^{1}H NMR of THF reaction of **8**-d_1/**9**-d_1 (400.1 MHz, $CDCl_3$, 25 °C): δ 4.3 (0.2 H as compared to 3H methoxy signals at ca. δ 3.8). The ee was determined to be 69% (*R*). ^{1}H NMR of MeOH reaction of **8**-d_1/**9**-d_1 (400.1 MHz, $CDCl_3$, 25 °C): δ 4.3 (0.15 H as compared to 3H methoxy signals at ca. δ 3.8). The ee was determined to be 70% (*R*). ^{1}H NMR of THF reaction of **10**-d_1 (400.1 MHz, $CDCl_3$, 25 °C): δ 4.2 (0.2 H as compared to 3H methoxy signals at ca. δ 3.8). The ee was determined to be 84% (*R*). ^{1}H NMR of MeOH reaction of **10**-d_1 (400.1 MHz, $CDCl_3$, 25 °C): δ 4.3 (0.1 H as compared to 3 H methoxy signals at ca. δ 3.8). The ee was determined to be 84% (*R*).

Reaction of [Ru((*R*)-BINAP)(MeCN)(OC(D)(CO_2R)(C(CH_3)$_2$-(CO_2R)))](BF_4) (5-d_1/6-d_1, 8-d_1/9-d_1, and 10-d_1) with HBF_4·OEt_2. The ruthenium−alkoxide complexes (**5**-d_1/**6**-d_1) (150.4 mg, 1.44×10^{-4} mol) were transferred to a 50 mL sidearm. The flask was sealed, placed under reduced pressure, and refilled (×3) to remove all traces of oxygen. To the flask was added CH_2Cl_2 (5.0 mL) via gastight syringe. The solution was stirred under argon atmosphere for 2 min. To this solution was added 1 equiv of HBF_4·OEt_2 via gastight syringe, resulting in an immediate color change from a deep orange to a pale yellow. The solution was stirred for 5 min then the flask was placed under reduced pressure to remove the solvent. The residue was analyzed by ^{1}H, ^{2}H, and ^{31}P NMR and determined to have produced the desired alcohol product, with complete retention of deuterium at the alkoxy position, and the [Ru((*R*)-BINAP)($MeCN)_4$](BF_4)$_2$ byproduct. The sample was passed through a Florisil plug with Et_2O and the solvent removed, and the product residue **11**-d_1 was analyzed for the enantiomeric excess (58% ee (*R*)). Similar reactions were performed with the ruthenium−alkoxides **8**-d_1/**9**-d_1 and with the ruthenium−alkoxide **10**. Reaction with **8**-d_1/**9**-d_1 yielded 79% ee (*R*), and reaction with **10**-d_1 yielded >99% ee (*R*).

Acknowledgment. We sincerely appreciate the expert assistance of Mr. G. Bigam and Dr. T. Nakashima of the University of Alberta High Field NMR Laboratory. We also thank the Natural Sciences and Engineering Research Council of Canada and the University of Alberta for financial support.

JA0102991